

Time series analysis of long-term photometry of BM Canum Venaticorum ^{*}

L. Siltala¹, L. Jetsu¹, T. Hackman¹, G.W. Henry², L. Immonen¹, P. Kajatkari¹, J. Lankinen¹, J. Lehtinen¹, S. Monira¹, S. Nikbakhsh¹, A. Viitanen¹, J. Viuhon¹, and T. Willamo¹

¹ Department of Physics, P.O. Box 64, FI-00014 University of Helsinki, Finland

² Center of Excellence in Information Systems, Tennessee State University, 3500 John A. Merritt Blvd., Box 9501, Nashville, TN 37209, USA

Received / Accepted

Key words Methods: data analysis, Stars: activity, binaries, starspots, individual (BM CVn)

We study standard Johnson differential V photometry of the RS CVn binary BM CVn spanning over a quarter of a century. Our main aims are to determine the activity cycles, the rate of surface differential rotation and the rotation period of the active longitudes of BM CVn. The Continuous Period Search (CPS) is applied to the photometry. The changes of the mean and amplitude of the light curves are used to search for activity cycles. The rotation period changes give an estimate of the rate of surface differential rotation. The Kuiper method is applied to the epochs of the primary and secondary minima to search for active longitudes. The photometry reveals the presence of a stable mean light curve (MLC) connected to the orbital period $P_{\text{orb}} = 20^{\text{d}}6252$ of this binary. We remove this MLC from the original V magnitudes which gives us the corrected V' magnitudes. These two samples of V and V' data are analysed separately with CPS. The fraction of unreliable CPS models decreases when the MLC is removed. The same significant activity cycle of approximately 12.5 years is detected in both V and V' samples. The estimate for the surface differential rotation coefficient, $k \geq 0.10$, is the same for both samples, but the number of unrealistic period estimates decreases after removing the MLC. The same active longitude period of $P_{\text{al}} = 20^{\text{d}}511 \pm 0^{\text{d}}005$ is detected in the V and V' magnitudes. This long-term regularity in the epochs of primary and secondary minima of the light curves is not caused by the MLC. On the contrary, the MLC hampers the detection of active longitudes.

Copyright line will be provided by the publisher

1 Introduction

Bidelman (1983) noticed the strong Ca II K line emission of BM CVn (HD116204, BD+39 2635). Hall (1983) suspected photometric variability. This was confirmed by Boyd et al. (1984), who discovered a period of $P_{\text{phot}} = 21^{\text{d}}3$ from a light curve having an amplitude of $0^{\text{m}}07$. Furthermore, Boyd et al. (1984) suggested that BM CVn is a RS CVn binary. Among other published P_{phot} values are $21^{\text{d}}9$ (Mohin & Raveendran, 1987), $20^{\text{d}}66 \pm 0^{\text{d}}03$ (Strassmeier et al., 1989) and $20^{\text{d}}2 \pm 0^{\text{d}}5$ (Erdem et al., 2009). However, Koen & Eyer (2002) detected no periodicity in the Hipparcos photometry of $n = 169$ observations.

Griffin & Fekel (1988) showed that BM CVn is a binary with $P_{\text{orb}} = 20^{\text{d}}6252 \pm 0^{\text{d}}0018$, and noted that the secondary companion could not be detected spectroscopically. BM CVn is currently classified as a single-lined eclipsing binary with $v \sin i = 15$ km/s in the Third catalogue of chromospherically active binaries (Eker et al., 2008). The suggested spectral types of the primary are K3 III (Simon & Fekel, 1987), KI III (Sato & Kuji, 1990) and G8 III (Boffin et al.,

1993). Mohin & Raveendran (1987) arrived at a lower limit estimate, $R \geq 6R_{\odot}$, for the primary. Stawikowski & Glebocki (1994) argued that the inclination of the orbital plane, $i_{\text{orb}} = 26^{\circ}$, is nearly equal to the inclination of the rotation axis of the primary, $i_{\text{rot}} = 24^{\circ}$. Their estimate for the primary radius was $15 \pm 2R_{\odot}$.

Activity induced chromospheric or coronal emission of BM CVn has been detected in the optical Ca II H&K and H α lines, as well as in UV and X-ray wavelengths (Dempsey et al., 1993; Fekel et al., 1986; Frasca & Catalano, 1994; Montes et al., 2000; Pérez Martínez et al., 2011; Sato & Kuji, 1990; Strassmeier et al., 1990). Radio and IR emission has also been detected (Haakonsen & Rutledge, 2009; Helfand et al., 1999; Mitrou et al., 1996).

Recent studies have shown that for some RS CVn binaries the light curve is heavily biased by the ellipsoidal shape of the primary (Roettenbacher et al., 2015a,b). Furthermore, other physical processes, e.g. mass transfer between close binaries could distort the light curve. These kinds of distortions would always follow the periodicity of the orbital period. Long-term active longitudes, on the other hand, may follow a different periodicity (Hackman et al., 2011). Thus, if the difference between these periods is large enough, we can separate the spot activity from other variability connected to the orbital period. One way to attempt this is to subtract a mean light curve fit calculated with the

^{*} The analysed photometry and numerical results of the analysis are both published electronically at the CDS via anonymous ftp to cdsarc.u-strasbg.fr (130.79.128.5) or via <http://cdsarc.u-strasbg.fr/viz-bin/qcat?J/A+A/yyy/Axxx>

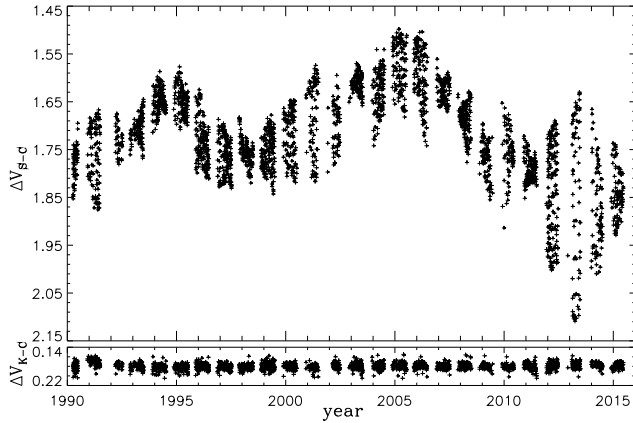


Fig. 1 Photometric data. Upper panel: All ΔV_{S-C} data. Lower panel: All ΔV_{K-C} data in the same magnitude scale as in the upper panel

orbital period. This approach is, in a sense, similar to the pre-whitening used in detecting stellar differential rotation (Reinhold et al., 2013).

In the current study, we apply the Continuous Period Search (Lehtinen et al., 2011, CPS) to photometry of BM CVn spanning over a quarter of a century. One of our aims is to look for active longitudes. Therefore we check whether the binary has any orbital period mean light curve, which could distort the detection of active longitudes.

2 Observations

Our differential photometry was obtained with the T3 0.4m automated photoelectric telescope (APT) at Fairborn Observatory in Arizona. The observations were made between April 6th, 1990 (HJD = 2447987.9) and June 15th, 2015 (HJD = 2457188.8). The comparison and check stars of our target star, S = BM CVn, were C = HD 116010 (Yoss & Griffin, 1997, K2II-III, $V=5.60$) and K = HD 115271 (Royer et al., 2007, A7V, $V = 5.78$). The mean (m) and the standard deviation (s) of standard Johnson differential magnitudes, ΔV_{S-C} (Fig. 1, upper panel: $n = 2930$), were $m \pm s = 1^m721 \pm 0^m096$. The respective values for the ΔV_{K-C} differential magnitudes (Fig. 1, lower panel: $n = 2744$) were $m \pm s = 0^m1797 \pm 0^m0064$. Hence, C = HD 116010 was a reliable comparison star, the accuracy of our photometry was approximately $\sigma_V = 0^m0064$, and the observed variations of S = BM CVn were certainly real. The photometric data reduction procedures and the operation of the T3 0.4 m APT have been described in detail, e.g., by Henry (1999) and Fekel & Henry (2005). The differential ΔV_{S-C} magnitudes are hereafter referred to as the original V magnitudes.

3 CPS method

We analysed the original V magnitudes of BM CVn with the CPS method formulated by Lehtinen et al. (2011). This

method is described here only briefly, because we have already applied it to the photometry of numerous stars (Hackman et al., 2011, 2013; Kajatkari et al., 2014, 2015; Lehtinen et al., 2011, 2012, 2016). We divided the observations into datasets having a maximum length of $\Delta T_{\max} = 1.5P_{\text{orb}} = 30^d94$. The modelled datasets contained at least $n \geq n_{\min} = 14$ observations. CPS uses a sliding window with a length of ΔT_{\max} and models all datasets having at least n_{\min} observations within such a window. The notation for the mean of the n observing times t_i of a dataset is τ . The CPS model is

$$\hat{y}(t_i) = \hat{y}(t_i, \vec{\beta}) = M + \sum_{k=1}^K [B_k \cos(k2\pi f t_i) + C_k \sin(k2\pi f t_i)],$$

where K is the model order and $\vec{\beta} = [M, B_1, \dots, B_K, C_1, \dots, C_K, f]$ is vector of free parameters. The best modelling order K for each dataset is chosen by using a Bayesian criterion (Lehtinen et al., 2011, Eq. 6). Here, the tested orders for this best model were $0 \leq K \leq 2$. These models gave the following physically meaningful light curve parameters: the period $P(\tau)$, the mean brightness $M(\tau)$, the peak to peak amplitude $A(\tau)$, and the epochs of the primary and secondary minima in time, $t_{\min,1}(\tau)$ and $t_{\min,2}(\tau)$. The error estimates for these light curve parameters were determined with the bootstrap method (Lehtinen et al., 2011). The reliable and unreliable parameter estimates were identified from these bootstrap results. The parameter estimates were considered reliable if the distribution of the bootstrap estimates for all model parameters and the model residuals followed a Gaussian distribution (Lehtinen et al., 2011). Two concrete examples of the use of this reliability criterion can be found in (Jetsu & Pelt, 1999, Figs. 2 and 4). We use the notation $R(\tau) = 0$ for the reliable light curve parameter estimates and $R(\tau) = 1$ for the unreliable ones. The modelling results correlate for temporally overlapping subsets containing common data. We selected a sequence of independent datasets which did not overlap. The notation for these independent datasets is $\text{IND}(\tau) = 1$, while that for the remaining overlapping datasets with common data is $\text{IND}(\tau) = 0$.

4 Analysis of V magnitudes

4.1 CPS results for the original V magnitudes

We detected periodicity in all 1319 original V magnitude datasets. The order of the best model was $K = 1$ in 205 datasets and $K = 2$ in 1114 datasets. CPS gave the following numbers of different types of $M(\tau)$, $A(\tau)$, $P(\tau)$, $t_{\min,1}(\tau)$ and $t_{\min,2}(\tau)$ estimates:

	IND(τ)=1 R(τ)=0	IND(τ)=1 R(τ)=1	IND(τ)=0 R(τ)=0	IND(τ)=0 R(τ)=1
$M(\tau)$	$n = 107$ [■]	$n = 12$ [□]	$n = 1098$ [×]	$n = 102$ [×]
$A(\tau)$	$n = 107$ [■]	$n = 12$ [□]	$n = 1098$ [×]	$n = 102$ [×]
$P(\tau)$	$n = 107$ [■]	$n = 12$ [□]	$n = 1098$ [×]	$n = 102$ [×]
$t_{\min,1}(\tau)$	$n = 107$ [■]	$n = 12$ [□]	$n = 1098$ [×]	$n = 102$ [×]
$t_{\min,2}(\tau)$	$n = 23$ [▲]	$n = 6$ [△]	$n = 293$ [×]	$n = 42$ [×]

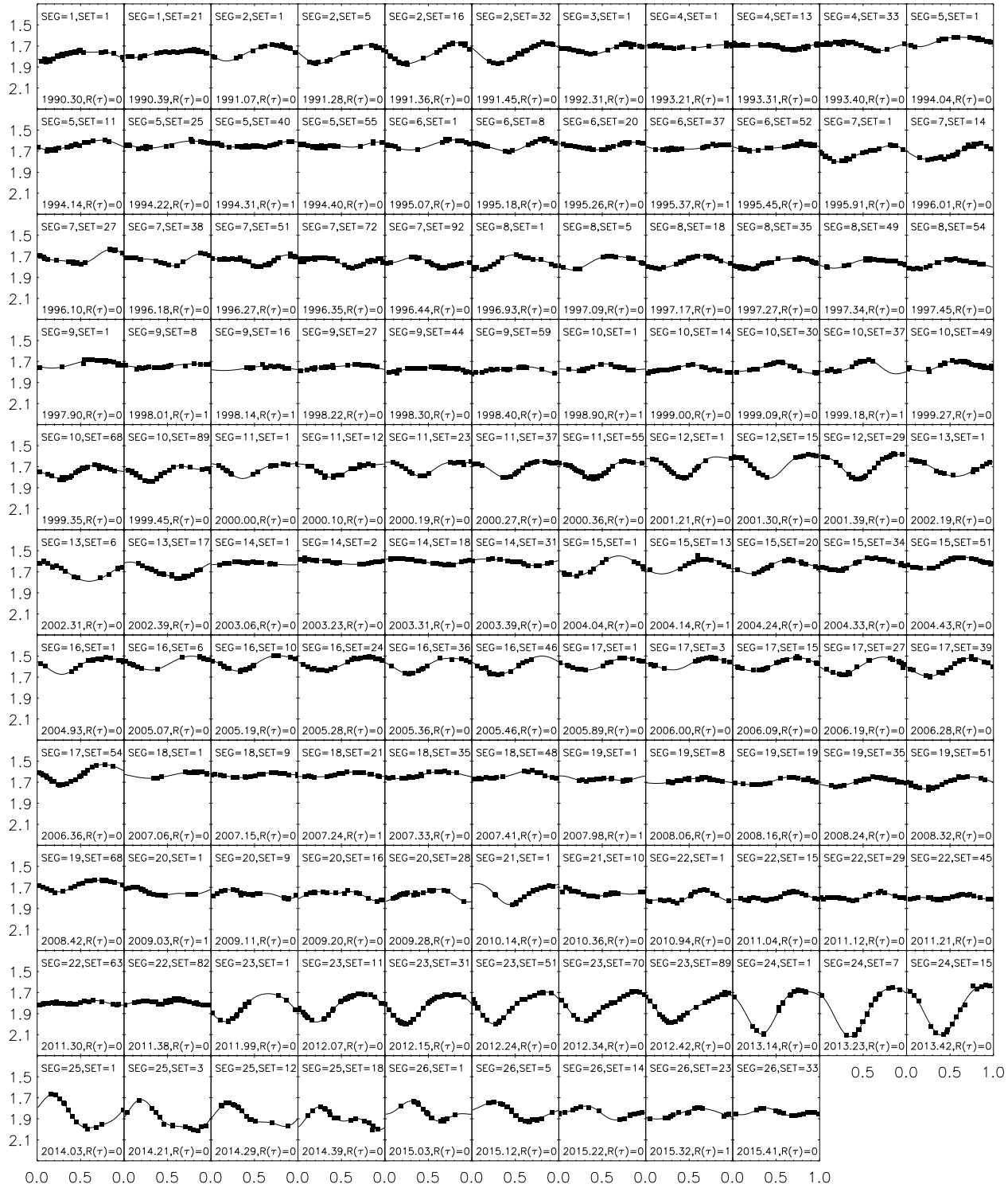


Fig. 2 The data and the light curves of 119 independent V magnitude datasets ($\text{IND}(\tau = 1)$). The reliable and unreliable models are denoted with $R(\tau) = 0$ and 1 , respectively. The x-axis is the phase ϕ and the y-axis is the magnitude V . The computation of the phases ϕ is explained in the last paragraph of Sect. 4.1.

Note that the symbols given in the brackets are those used in Figs. 3–6 for the modelling results of the original V magnitude data. All CPS analysis results for the independent V datasets are published electronically at the CDS.

The data and the CPS models of the 119 independent datasets are shown in Fig. 2. We first computed the phases $\phi_1 = \text{FRAC}[(t - t_{\min,1}(\tau))/P(\tau)]$, where $\text{FRAC}[x]$ removes the integer part of its argument x . Then, the phases $\phi_{al,1}$ of the primary minima $t_{\min,1}(\tau)$ were computed with the active longitude ephemeris of Eq. 2. The photometry and the CPS models are plotted as a function of the phase $\phi = \phi_1 + \phi_{al,1}$ in Fig. 2.

4.2 Activity cycles in V photometry

Horne & Baliunas (1986) formulated the power spectrum method (hereafter PSM) which was applied by Baliunas et al. (1995) to search for activity cycles in the chromospheric Ca II H&K emission line data. For example, Rodonò et al. (2000) and Kajatkari et al. (2015) have applied PSM to the following light curve parameters: $M(\tau)$ (axisymmetric part of spot distribution), $A(\tau)$ (non-axisymmetric part of spot distribution), $M(\tau)+A(\tau)/2$ (maximum spottedness) or $M(\tau)-A(\tau)/2$ (minimum spottedness). These four parameters are also analysed here, although there are actually only two independent variables, $M(\tau)$ and $A(\tau)$. Furthermore, the amplitude of the light curve does not depend only on the area of the spots, but there are also other causes, e.g. variations of the temperature of the spots or the connection between their projected area and their latitude.

The $M(\tau)$ and $A(\tau)$ changes of BM CVn are shown in Figs. 3. PSM detected the following activity cycles P_c in the $n = 107$ independent and reliable estimates of the above four parameters of BM CVn, where F is the false alarm probability (Horne & Baliunas, 1986)

	$P_c \pm \sigma_{P_c}$	F
$M(\tau)$	$13^{\circ}1 \pm 0^{\circ}2$	5×10^{-11}
$A(\tau)$	$12^{\circ}0 \pm 0^{\circ}3$	2×10^{-4}
$M(\tau) + A(\tau)/2$	$12^{\circ}8 \pm 0^{\circ}2$	5×10^{-10}
$M(\tau) - A(\tau)/2$	$18^{\circ}2 \pm 0^{\circ}4$	7×10^{-9}

All F values indicate that these cycles are very significant. Considering the σ_{P_c} errors, the first three parameters may follow the same activity cycle of approximately $12^{\circ}5$ which has been repeated twice between 1990 and 2015. However, the parameter $M(\tau)-A(\tau)/2$ appears to follow another cycle of $18^{\circ}2$.

4.3 Differential rotation in V photometry

The $P(\tau)$ changes of BM CVn are shown in Fig. 4. Numerous unrealistic period estimates were obtained for low amplitude light curves, e.g. in the years 1992, 1993, 1995 and 1998. Our estimate for the differential rotation of BM CVn is based on the $n = 107$ reliable $P(\tau)$ estimates of independent datasets. We compute the value of the parameter

$$Z = 6\Delta P_w/P_w = 0.10 \equiv 10\%, \quad (1)$$

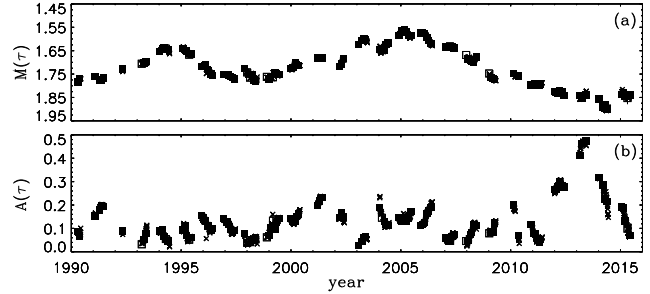


Fig. 3 a) Mean $M(\tau)$ for the original V magnitudes, b) Amplitude $A(\tau)$ for the original V magnitudes. The symbols are explained in the first paragraph of Sect. 4.1

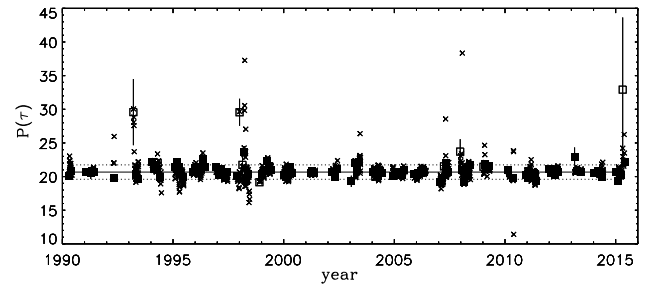


Fig. 4 Period $P(\tau)$ for the original V magnitudes. The P_w and $P_w \pm 3\Delta P_w$ levels are denoted with horizontal continuous and dotted lines, respectively.

where $P_i \pm \sigma_{P,i}$ is period of i :th dataset, $w_i = \sigma_{P,i}^{-2}$ is the weight, $P_w = [\sum_{i=1}^{107} w_i P_i] / [\sum_{i=1}^{107} w_i]$ is the weighted mean of P_i and $\Delta P_w = \{[\sum_{i=1}^{107} w_i (P_i - P_w)^2] / [\sum_{i=1}^{107} w_i]\}^{1/2}$ is the error of this weighted mean P_w (Lehtinen et al., 2011, Eq. 14). The numerical values for BM CVn are $P_w \pm \Delta P_w = 20^{\circ}67 \pm 0^{\circ}36$. We use the multiplying constant value of 6 in Eq. 1, because parameter Z is the $\pm 3\Delta P_w$ upper limit for the period variations.

Lehtinen et al. (2011, their Eq. 15) introduced the relation $Z_{\text{phys}} = Z^2 - Z_{\text{spu}}^2$, where Z measures the observed period changes of Eq. 1, while Z_{phys} and Z_{spu} measure the real physical and unreal spurious period changes. The mean of the half amplitude $A(\tau)/2$ of the above mentioned 107 models of BM CVn is $A_{\text{half}} = 0^{\circ}068$. The data precision is $N = \sigma_V = 0^{\circ}0064$. This yields a “signal to noise” ratio of $\epsilon = A_{\text{half}}/N \approx 10$. Together with the mean number of data points per dataset, $n_{\text{data}} = 19.9$, and the ratio of the mean rotation period to the dataset length, $n_{\text{rot}} = 1.45$, this predicts spurious changes of $Z_{\text{spu}} \approx 0.08$ (Lehtinen et al., 2016, Eq. 10). This is a major fraction of the raw estimate $Z = 0.10$, although the physically originating component of the period changes may still be estimated at $Z_{\text{phys}} \approx (Z^2 - Z_{\text{spu}}^2)^{1/2} = 0.06$.

One approximation for the solar law of differential rotation is $P(b) = P(b=0)/[1 - k_{\odot}(\sin b)^2]$, where b is the latitude and $k_{\odot} = 0.2$ is the solar differential rotation coefficient. If this law were valid for BM CVn and its $P(\tau)$ were reliable tracers of surface differential rotation, the differential rotation coefficient of BM CVn would be $|k| =$

Z_{phys}/h , where b_{min} and b_{max} are the minimum and maximum latitudes of spot activity, and $h = \sin^2 b_{\text{max}} - \sin^2 b_{\text{min}}$ (Jetsu et al., 2000). The exact latitudes of the spots can not be determined from photometric observations, and thus the numerical value of h remains unknown. For example, if spots form at all latitudes between the equator and pole of BM CVn, this coefficient reaches its maximum value $h = 1$. Thus, the relation $|k| > Z_{\text{phys}} \approx 0.06$ is valid for all possible b_{min} and b_{max} values.

4.4 Active longitudes in V photometry

The spots on the surface of rapidly rotating giants have been observed to concentrate on long-lived active longitudes (e.g. Jetsu, 1996). Such structures have been detected, e.g. with the nonweighted or weighted Kuiper test formulated in Jetsu & Pelt (1996, Sect. 3.1). In this test, the phases ϕ_i of n time points t_i are first computed with the tested period P . These phases are then arranged into increasing order (i.e. rank order). The monotonously increasing sample distribution function $F_n(\phi_i) = i/n$ of these phases is compared to the sample distribution function of an even distribution $F(\phi) = \phi$, i.e. a random distribution. The Kuiper test statistic is $V_n = D^+ + D^-$, where $D^+ = F_n(\phi) - F(\phi)$ and $D^- = F(\phi) - F_n(\phi)$. A large V_n value indicates that the phases ϕ_i do not represent a sample drawn from a random distribution, i.e. the phases ϕ_i are not evenly distributed and there is periodicity in time points t_i with the tested period P .

We applied the nonweighted Kuiper test to the reliable $t_{\text{min},1}(\tau)$ estimates of all independent datasets ($n = 107$). The tested period range was between $0.85P_w = 17^{\text{d}}.6$ and $1.15P_w = 23^{\text{d}}.8$. The best rotation period for the active longitudes of BM CVn was $P_{\text{al}} = 20^{\text{d}}.511 \pm 0^{\text{d}}.005$. This periodicity reached an extreme significance of $Q_K = 1 \times 10^{-7}$ (Jetsu & Pelt, 1996, Eq. 24). We also applied the same test to the reliable $t_{\text{min},1}(\tau)$ and $t_{\text{min},2}(\tau)$ estimates of all independent datasets ($n = 130$). The result was exactly the same, $20^{\text{d}}.511 \pm 0^{\text{d}}.008$ ($Q_K = 4 \times 10^{-7}$).

All $t_{\text{min},1}(\tau)$ and $t_{\text{min},2}(\tau)$ estimates of BM CVn are shown in Fig. 5. The phases are calculated from the active longitude ephemeris

$$\text{HJD}_0 = 2\,447\,987.8762 + 20^{\text{d}}.511\text{E}, \quad (2)$$

where the zero epoch is the time of the first photometric observation. The majority of the reliable primary minima of independent datasets concentrate between phases 0.1 and 0.6 (Fig. 5a: closed squares and Fig. 5b: dark areas). The corresponding simultaneous secondary minima are usually about half a rotation apart from these primary minima (Fig. 5a: closed triangles). The light curves had only one minimum in the years 1991–1992, 1997, 2001–2006, 2011–2013, i.e. two minima were present for half of the time. When the activity was present on both longitudes, the longitude with stronger activity determined the phase of $t_{\text{min},1}(\tau)$ (Fig. 5a: closed squares). Sometimes the activity shifted abruptly nearly to the opposite side of the stellar hemisphere, like in the years 2003–2004. This type of the “flip-flop”

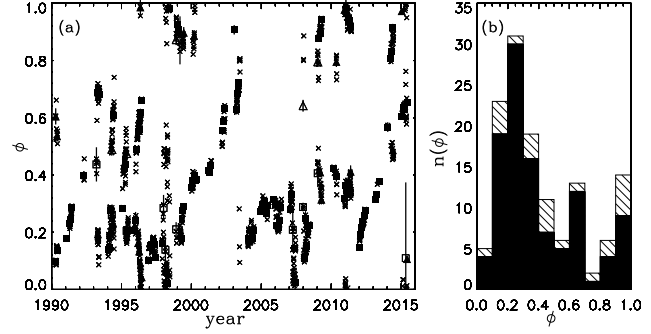


Fig. 5 (a) $t_{\text{min},1}(\tau)$ and $t_{\text{min},2}(\tau)$ for the original V magnitudes with the active longitude ephemeris of Eq. 2. (b) Histogram of the number of values $n(\phi)$ within 0.1 bins in phase. The dark and shaded areas denote the reliable $t_{\text{min},1}(\tau)$ and $t_{\text{min},2}(\tau)$ estimates of independent datasets, respectively.

events have previously been observed, e.g. on the rapidly rotating single G4 III giant FK Comae (Jetsu et al., 1993).

If the inclination of the primary were indeed only $i_{\text{rot}} = 24^\circ$ (Stawikowski & Glebocki, 1994), then extreme spot coverage would be required to explain the high amplitudes of $A(\tau) \approx 0^{\text{m}}.5$ in the year 2013 (Fig. 3).

Using the Barnes-Evans relation as formulated by Lacy (1977) we can derive an alternative estimate of the stellar radius with the formula

$$\log R/R_\odot = 7.4724 - 0.2V_0 - 2F_V + \log d \quad (3)$$

where $F_V = 3.977 - 0.429(V - R)_0$ and $[d] = pc$. The Hipparcos parallax of 8.86 mas (van Leeuwen, 2007) combined with the V magnitude and $V - R \approx 0.81$ (Eker et al., 2008) indicate a primary radius of $\sim 8R_\odot$. This would mean that the rotational inclination of the primary is in fact $i_{\text{rot}} \sim 50^\circ$. This value would still require a high, but not extreme spot coverage. Furthermore, assuming approximately the same orbital inclination, would result in a secondary mass of $\sim 0.3M_\odot$. Thus it is no surprise that its spectral lines have not been observed.

Recently, Roettenbacher et al. (2015b) showed that the ellipsoidal shape of the primary of another RS CVn binary σ Gem (Duemmler et al., 1997, $P_d = 19^{\text{d}}.604471 \pm 0^{\text{d}}.000022$) offered an alternative explanation for the active longitude hypothesis presented by Kajatkari et al. (2014). For BM CVn, the active longitude period $P_{\text{al}} = 20^{\text{d}}.511 \pm 0^{\text{d}}.005$ is only 0.55% smaller than the orbital period $P_{\text{orb}} = 20^{\text{d}}.6252 \pm 0^{\text{d}}.0018$. This period difference causes a $\Delta\phi = 2.48$ phase difference during the whole time span of data. The three periods of BM CVn increase in the order $P_{\text{al}} < P_{\text{orb}} < P_w$. The $P_w = 20^{\text{d}}.67$ error, $\Delta P_w = 0^{\text{d}}.36$, does not exclude the cases $P_w < P_{\text{orb}}$ or $P_w < P_{\text{al}}$. However, the accuracy of the other two periods excludes the case $P_{\text{al}} > P_{\text{orb}}$.

We decided to test the ellipsoidal primary shape hypothesis for BM CVn. The orbital period ephemeris in Griffin & Fekel (1988) was

$$\text{HJD}_0 = 2\,445\,252.12 + 20^{\text{d}}.6252\text{E}. \quad (4)$$

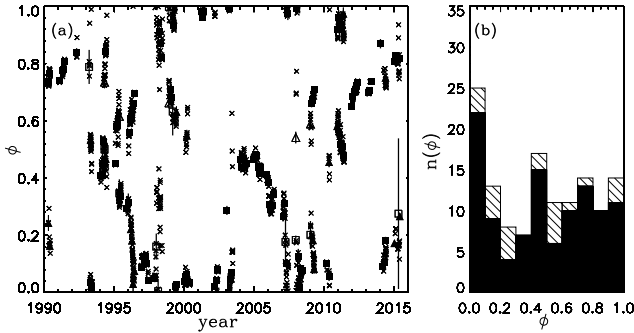


Fig. 6 $t_{\min,1}(\tau)$ and $t_{\min,2}(\tau)$ for the original V magnitudes with the orbital period ephemeris of Eq. 4. Otherwise as in Fig. 5.

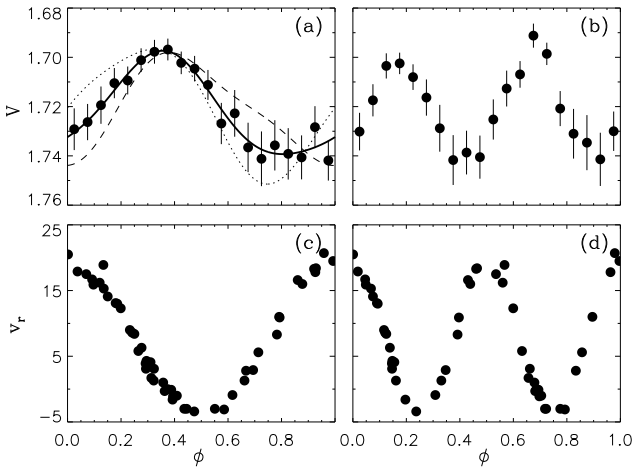


Fig. 7 (a) The MLC of BM CVn with the ephemeris Eq. 4. The bin width was 0.050 in phase ϕ . The error bars show the mean error within each bin. The continuous line shows the best fit with the model of Eqs. 5. The dashed and the dotted lines show the MLC for the binned data before and after the mid epoch 2002.85. (b) The MLC for the period $2P_{\text{orb}}$ in Eq. 4. (c) Radial velocities v_r in Griffin & Fekel (1988) with the ephemeris Eq. 4. (d) Same data for the period $2P_{\text{orb}}$ in Eq. 4.

The $t_{\min,1}(\tau)$ and $t_{\min,2}(\tau)$ phases of BM CVn computed with this ephemeris are shown in Fig. 6. These phases show no clear concentrations at $\phi = 0.25$ or 0.75 , which could be one signature of ellipticity. The minima of the binned B and V magnitude light curves of σ Gem were at these particular orbital phases in Roettenbacher et al. (2015b, their Fig. 5). The results of a similar binning of the V magnitudes of BM CVn are shown in Fig. 7a. This $0^{\text{m}}042$ peak to peak amplitude mean light curve (hereafter MLC) shows only one minimum and one maximum, while there were two maxima and minima in the MLC of σ Gem.

The MLC of BM CVn would also have two minima and maxima, if the real P_{orb} of BM CVn were two times larger than the one reported in Griffin & Fekel (1988) (Fig. 7b). However, this double period hypothesis must be rejected,

because the radial velocity measurements from Griffin & Fekel (1988) follow a single and double sine wave with P_{orb} and $2P_{\text{orb}}$, respectively (Figs. 7cd). These results do not support the ellipsoidal shape hypothesis, because the MLC of BM CVn does not have two minima and maxima. We will later discuss the possible cause of this sinusoidal MLC of BM CVn in the end of Sect. 6. Whatever the real cause may be, it is certain that this regular $0^{\text{m}}042$ variation has been misleading our CPS analysis of the original V magnitudes.

We also computed the MLC for the first and second part of the data, i.e. before and after the mid epoch of 2002.85. These two MLCs are denoted with dashed and dotted lines in Fig. 7a. Both of these curves show one maximum and minimum. The maximum deviation of both curves from the MLC of all data is only $0^{\text{m}}014$. The phase and the height of the MLC maximum of BM CVn has remained very stable, but the depth and the phase of the MLC minimum has varied. These MLC minimum variations are at least partly caused by the high amplitude light curves of the years 2012 and 2013. However, the MLC of BM CVn in Fig. 7a (continuous line) must be a real phenomenon, because the erratic changes of the light curve mean, amplitude and period, and especially those of the minimum and maximum phases, should cause a constant long-term MLC. The MLC was computed with P_{orb} . This induces a phase difference of $\Delta\phi = 2.48$ with P_{al} during the whole time span of data. Hence, the observed MLC phase coherence is not caused by active longitudes.

4.5 MLC corrected V' magnitudes

We used the Bayesian criterion from Lehtinen et al. (2011, Eq. 6) to determine the best modelling order K for the binned V magnitudes of Fig. 7a. The tested orders were $0 \leq K \leq 4$. The best order was $K = 2$. Hence, we modelled these binned V magnitudes with

$$g_2(\phi, \bar{\beta}_{\text{MLC}}) = a_0 + a_1 \cos(2\pi\phi) + b_1 \sin(2\pi\phi) + a_2 \cos(4\pi\phi) + b_2 \sin(4\pi\phi). \quad (5)$$

where the free parameters were $\bar{\beta}_{\text{MLC}} = [a_0, a_1, b_1, a_2, b_2]$ and the orbital phases ϕ were calculated from the ephemeris of Eq. 4. The best fit had $a_0 = 1.721 \pm 0.002$, $a_1 = 0.011 \pm 0.002$, $b_1 = -0.017 \pm 0.003$, $a_2 = 0.000 \pm 0.002$ and $b_2 = 0.003 \pm 0.002$. The continuous line outlines this model in Fig. 7a. The Bayesian criterion from Lehtinen et al. (2011, Eq. 6) revealed that a second order component was present in the MLC, although the amplitude of this second order part was low, i.e. constant a_2 was zero and constant b_2 was very close to zero. We used this same criterion to determine the best K value for the CPS models of *all* V and V' datasets.

This best fit of Eq. 5 was used to remove the MLC from the V magnitudes of BM CVn. The corrected magnitudes were computed from

$$V'(t_i) = V(t_i) - g_2(\phi, \bar{\beta}_{\text{MLC}}) + a_0 \quad (6)$$

where $V(t_i)$ were the original data and the values of the free parameters $\bar{\beta}_{\text{MLC}}$ were those of this best fit of Eq. 5. The

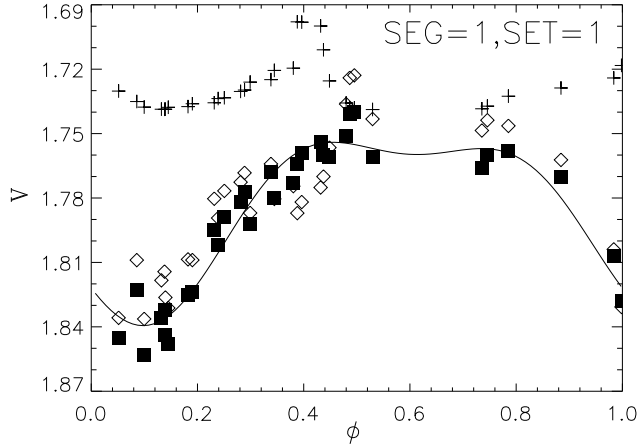


Fig. 8 An example of the MLC correction procedure. The data (closed squares) and the CPS model (continuous line) are from Fig. 2 (SEG=1, SET=1). The crosses denote MLC magnitudes computed from Eq. 5. The diamonds show the MLC corrected V' magnitudes (Eq. 6).

CPS analysis results do not depend on subtracting a constant value from differential photometry. Therefore, we did not subtract the MLC mean, i.e. the constant $a_0 = 1.721$, from the $V(t_i)$ data. In other words, a_0 was “added back” in Eq. 6.

One example of this correction procedure of Eqs. 5 and 6 is displayed in Fig. 8. The original V data are denoted with closed squares (SEG = 1, SET = 1). The continuous line shows the light curve for these original data, i.e. the first light curve from Fig. 2. The MLC values $g_2(\phi, \beta_{\text{MLC}})$ computed with Eq. 5 are scattered (Fig. 8: crosses). The reason for this scatter is that these MLC values are computed with the period $P_{\text{orb}} = 20^{\text{d}}6252$, but the correct period for these data is much shorter $P(\tau) = 20^{\text{d}}14 \pm 0^{\text{d}}31$. This mixes the MLC phases when these phases are computed “incorrectly” with $P(\tau)$, i.e. not with the correct period P_{orb} . The upward peak in the MLC values (crosses) close to phase 0.35 provides a nice example of the correction procedure. When this peak is subtracted from the original V data (closed squares), the corrected V' data show a dip at the same phase (open diamonds).

5 Analysis of V' magnitudes

5.1 CPS results for the MLC corrected V' magnitudes

We use a prime (') to denote all CPS analysis results for the V' magnitudes, e.g. $M'(\tau)$ for the mean. For τ , this notation is not required, because the observing times t_i of the $V(t_i)$ and $V'(t_i)$ magnitudes are the same. The total number of CPS models for the corrected V' magnitudes was 1319. Again, CPS detected periodicity in all datasets. The order of the best model was $K' = 1$ in 220 datasets and $K' = 2$ in 1099 datasets. The number of different types of CPS pa-

parameter estimates, $M'(\tau)$, $A'(\tau)$, $P'(\tau)$, $t'_{\text{min},1}(\tau)$ and $t'_{\text{min},2}(\tau)$, were:

	IND'(τ)=1 R'(τ)=0	IND'(τ)=1 R'(τ)=1	IND'(τ)=0 R'(τ)=0	IND'(τ)=0 R'(τ)=1
$M'(\tau)$	$n' = 105$ [■]	$n' = 14$ [□]	$n' = 1117$ [×]	$n' = 83$ [×]
$A'(\tau)$	$n' = 105$ [■]	$n' = 14$ [□]	$n' = 1117$ [×]	$n' = 83$ [×]
$P'(\tau)$	$n' = 105$ [■]	$n' = 14$ [□]	$n' = 1117$ [×]	$n' = 83$ [×]
$t'_{\text{min},1}(\tau)$	$n' = 105$ [■]	$n' = 14$ [□]	$n' = 1117$ [×]	$n' = 83$ [×]
$t'_{\text{min},2}(\tau)$	$n' = 24$ [▲]	$n' = 5$ [△]	$n' = 321$ [×]	$n' = 33$ [×]

The symbols used for the modelling results of these parameters in Figs. 10–12 are given above in the brackets. The fraction of unreliable CPS models was $114/1319 = 8.6\%$ for the original V magnitudes. This fraction decreased to $97/1319 = 7.4\%$ for the V' magnitudes. Hence, the number of reliable models ($R'(\tau) = 0$) increased when the MLC was removed from the original V magnitudes. The CPS analysis results of the corrected V' magnitudes are also published only electronically at the CDS.

The CPS models of 119 independent V' magnitude datasets are shown in Fig. 9. The phases were first computed from $\phi'_1 = \text{FRAC}[(t - t'_{\text{min},1}(\tau))/P'(\tau)]$. Then, we computed the phases $\phi'_{al,1}$ of the primary minima $t'_{\text{min},1}(\tau)$ with the active longitude ephemeris of Eq. 2. The V' magnitudes and the CPS models are plotted as a function of the phase $\phi' = \phi'_1 + \phi'_{al,1}$ in Fig. 9. The light curves of the original V and corrected V' magnitudes are nearly identical (Figs. 2 and 9). The largest change in the mean values $M(\tau)$ and $M'(\tau)$ is $0.^{\text{m}}014$. It occurs in SET=18 of SEG 11. The largest amplitude change, $0.^{\text{m}}027$, between $A(\tau)$ and $A'(\tau)$ occurs in SET=1, SEG=19. The light curves of this latter dataset are displayed in Figs. 2 and 9.

5.2 Activity cycles in V' photometry

The amplitude of the MLC was low, i.e. only $0.^{\text{m}}042$. Hence, the correction of Eq. 6 should not cause large changes in the mean and amplitude of the CPS light curves. The maximum differences were $\max(|M(\tau) - M'(\tau)|) = 0.^{\text{m}}014$ and $\max(|A(\tau) - A'(\tau)|) = 0.^{\text{m}}027$. When we applied PSM to the corresponding CPS parameters as in Sect. 4.2, the results were

	$P'_c \pm \sigma'_{P_c}$	F'
$M'(\tau)$	$13^{\text{y}}1 \pm 0^{\text{y}}2$	1×10^{-10}
$A'(\tau)$	$12^{\text{y}}0 \pm 0^{\text{y}}3$	5×10^{-4}
$M'(\tau) + A'(\tau)/2$	$12^{\text{y}}9 \pm 0^{\text{y}}2$	2×10^{-10}
$M'(\tau) - A'(\tau)/2$	$18^{\text{y}}2 \pm 0^{\text{y}}4$	5×10^{-9}

The best cycles were practically the same as those for the original V magnitudes. All this supported the presence of an activity cycle of approximately $12^{\text{y}}.5$.

5.3 Differential rotation in V' photometry

The results for $P'(\tau)$ are shown in Fig. 11. The $n' = 105$ independent and reliable period estimates had $P'_w \pm \Delta P'_w =$

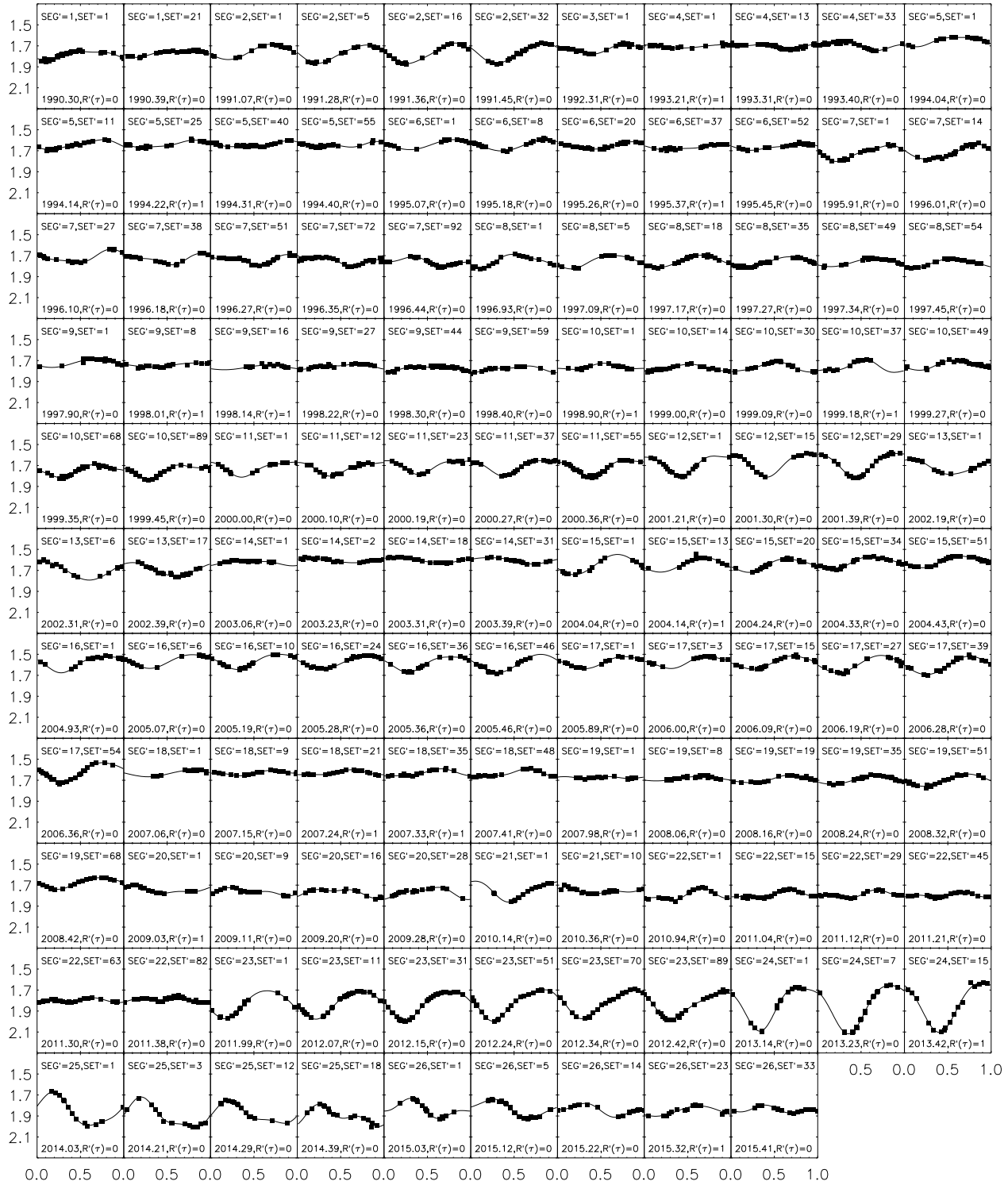


Fig. 9 The light curves of 119 independent V' magnitude datasets ($IND'(\tau = 1)$). The reliable and unreliable models are denoted with $R'(\tau) = 0$ and 1, respectively. The x-axis is the phase ϕ and the y-axis is the magnitude V' . The computation of phases ϕ is explained the last paragraph of Sect 5.1.

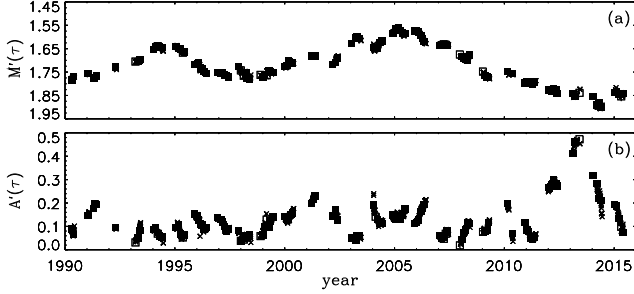


Fig. 10 **a)** Mean $M'(\tau)$ for the V' magnitudes. **b)** Amplitude $A'(\tau)$ for the V' magnitudes. The symbols are explained in the first paragraph of Sect. 5.1

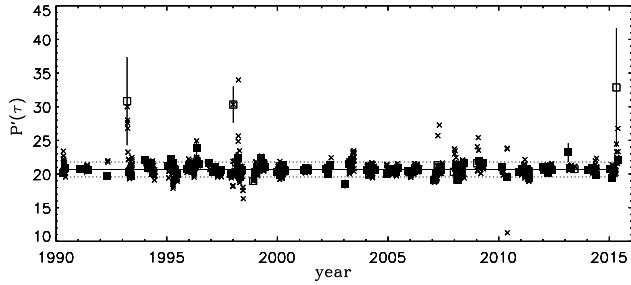


Fig. 11 Period $P'(\tau)$ for the corrected V' magnitudes, otherwise as in Fig. 4

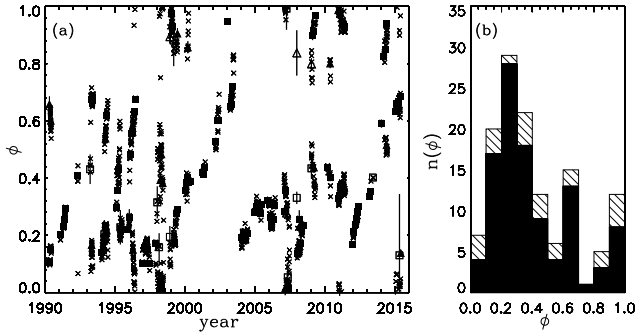


Fig. 12 $t'_{\min,1}(\tau)$ and $t'_{\min,2}(\tau)$ for the corrected V' magnitudes with active longitude ephemeris of Eq. 2.

$20^{\text{d}}67 \pm 0^{\text{d}}37$, which was equal to $Z' = 0.11 \equiv 11\%$. The signal to noise ratio A/N was practically the same as for the original V magnitude data, because there were no significant changes in the light curve amplitudes. Hence, the V' magnitude data gave close to the same differential rotation coefficient estimate $k' \geq Z'_{\text{phys}} = 0.08$ (with changes $Z_{\text{spu}} = 0.08$). Comparison of Figs. 4 and 11 revealed that the MLC correction eliminated numerous unrealistic $P(\tau)$ values obtained in the CPS analysis of original V magnitudes. Most of the remaining unrealistic $P'(\tau)$ values were obtained during the year 1998 when the amplitude $A'(\tau)$ of light curves was very close to zero.

5.4 Active longitudes in V' photometry

The nonweighted Kuiper test was applied to the $n' = 105$ reliable $t'_{\min,1}(\tau)$ estimates of independent datasets. The tested

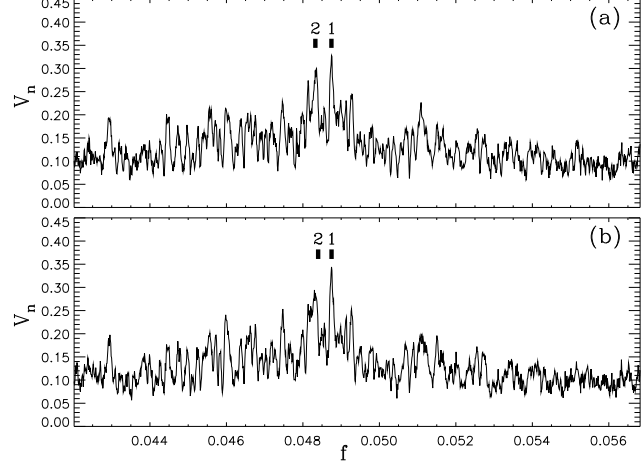


Fig. 13 **a)** Kuiper periodogram for the $n = 107$ independent and reliable $t_{\min,1}(\tau)$ estimates of original V magnitudes. The thick horizontal lines denote the locations of the two best periods $1 \equiv 20^{\text{d}}51$ and $2 \equiv 20^{\text{d}}68$. **b)** Kuiper periodogram for the $n' = 105$ independent and reliable $t'_{\min,1}(\tau)$ estimates of corrected V' magnitudes. The two best periods are $1 \equiv 20^{\text{d}}51$ and $2 \equiv 20^{\text{d}}70$.

period range was the same as in Sect. 4.4. The best active longitude rotation period was $P'_{\text{al}} = 20^{\text{d}}512 \pm 0^{\text{d}}005$ ($Q_K = 5 \times 10^{-8}$). The result for the $n' = 129$ reliable $t'_{\min,1}(\tau)$ and $t'_{\min,2}(\tau)$ estimates of independent datasets was the same, $20^{\text{d}}512 \pm 0^{\text{d}}010$ ($Q_K = 6 \times 10^{-7}$). The P_{al} and P'_{al} values were also the same within their error limits. Therefore, the ephemeris of Eq. 2 was also used in our Fig. 12, which shows the phases of $t'_{\min,1}(\tau)$ and $t'_{\min,2}(\tau)$. Most of the reliable $t'_{\min,1}(\tau)$ estimates of independent datasets concentrate between phases 0.1 and 0.7.

The Kuiper test periodograms V_n for the primary minima of the original V magnitudes and the corrected V' magnitudes are shown in Figs. 13. The two best active longitude periods for the original V magnitudes were $20^{\text{d}}51$ ($Q_K = 1 \times 10^{-7}$) and $20^{\text{d}}68$ ($Q_K = 1 \times 10^{-5}$). The V_n peak of the second best period value in Fig. 13a was also very significant. The two best active longitude periods for the corrected V' magnitudes were $20^{\text{d}}51$ ($Q_K = 5 \times 10^{-8}$) and $20^{\text{d}}70$ ($Q_K = 4 \times 10^{-5}$) (Fig. 13b). After the MLC correction, the significance of the best period increased, while the significance of the second best period decreased. From this we could conclude that the MLC did not cause the active longitudes. On the contrary, the MLC hampered the detection of active longitudes.

6 Conclusions

We analysed a quarter of a century of photometry of BM CVn. The original V magnitude data were binned as a function of phase computed with the orbital period ephemeris of Eq. 4. This revealed that the photometry contained a mean light curve, or MLC, having a peak to peak amplitude of

0^m042 (Fig. 7a). The corrected V' magnitudes were computed by subtracting the MLC from the original V magnitudes (Eq. 6)

The Continuous Period Search, or CPS, algorithm was applied to the original V magnitudes and the corrected V' magnitudes. When we removed the MLC from the data, the fraction of unreliable CPS models decreased from 8.6% to 7.4%. The same activity cycle of approximately 12.5 years was detected with the power spectrum method from the V and V' magnitudes (Sects. 4.2 and 5.2). The results for the differential rotation coefficient were nearly the same for the V and V' magnitudes, $k \geq Z_{\text{phys}} = 0.06$ and $k' \geq Z'_{\text{phys}} = 0.08$ (Sects. 4.3 and 5.3). However, the number of unrealistic period estimates decreased after the MLC was removed (Figs. 4 and 11). It has to be noted that the estimated level of spurious period changes at $Z_{\text{spu}} = 0.08$ is significant due to the long rotation period of the star in relation to reasonable dataset lengths. Thus the estimated differential rotation values have considerable uncertainties. The same active longitude rotation period, $P_{\text{al}} = 20^{\text{d}}511 \pm 0^{\text{d}}005$, was detected with the nonweighted Kuiper method from the primary minima of V and V' data (Eq. 2). This result did not change when the secondary minima were also included into the analysis (Sects. 4.4 and 5.4). We showed that the MLC hampered the detection of active longitudes. Hence, the MLC was certainly not the cause for observing such long-term regularities in the light curve minima of BM CVn.

The ellipticity of the primary component of another RS CVn star, σ Gem, causes a regular MLC as a function of the orbital period (Roettenbacher et al., 2015b). Due to projection effects, this MLC has two minima and maxima. Roettenbacher et al. (2015b) argued that this MLC may be the reason for observing two active longitudes in σ Gem, i.e. this phenomenon may not be connected to dark spots or to chromospheric activity in general. The MLC of BM CVn has only one minimum and one maximum (Fig. 7) and ellipticity cannot therefore be the cause for this regularity. Innumerable different types of light curves have been observed in different classes of variable stars (e.g. Drake et al., 2014). For example, a mass transfer induced bright spot in BM CVn could explain the observed MLC. If the rate of this mass transfer varies, the brightness changes caused by the bright spot also vary, and our MLC correction of Eq. 6 cannot remove such irregularity from the original V magnitude data. Nevertheless, we stress that the removal of the MLC increased the detectability of the active longitudes. This is an indication of the MLC being caused by physics unrelated to spot activity.

Acknowledgements. This research at the Department of Physics (University of Helsinki) was performed in collaboration with the participants of the course Variable stars, which was lectured in autumn 2014. We have made use of the SIMBAD database at CDS, Strasbourg, France and NASA's Astrophysics Data System (ADS) bibliographic services. The automated astronomy program at Tennessee State University has been supported by NASA, NSF, TSU and the State of Tennessee through the Centers of Excellence program.

References

- Baliunas, S. L., Donahue, R. A., Soon, W. H., et al. 1995, *ApJ*, 438, 269
- Bidelman, W. P. 1983, *AJ*, 88, 1182
- Boffin, H. M. J., Cerf, N., & Paulus, G. 1993, *A&A*, 271, 125
- Boyd, L. J., Genet, R. M., & Hall, D. S. 1984, *Information Bulletin on Variable Stars*, 2546, 1
- Dempsey, R. C., Linsky, J. L., Fleming, T. A., & Schmitt, J. H. M. M. 1993, *ApJS*, 86, 599
- Drake, A. J., Graham, M. J., Djorgovski, S. G., et al. 2014, *ApJS*, 213, 9
- Duemmler, R., Ilyin, I. V., & Tuominen, I. 1997, *A&AS*, 123, 209
- Eker, Z., Ak, N. F., Bilir, S., et al. 2008, *MNRAS*, 389, 1722
- Erdem, A., Budding, E., Soydugan, E., et al. 2009, *New A*, 14, 545
- Fekel, F. C. & Henry, G. W. 2005, *AJ*, 129, 1669
- Fekel, F. C., Moffett, T. J., & Henry, G. W. 1986, *ApJS*, 60, 551
- Frasca, A. & Catalano, S. 1994, *A&A*, 284, 883
- Griffin, R. F. & Fekel, F. C. 1988, *Journal of Astrophysics and Astronomy*, 9, 213
- Haakonsen, C. B. & Rutledge, R. E. 2009, *ApJS*, 184, 138
- Hackman, T., Mantere, M. J., Jetsu, L., et al. 2011, *Astronomische Nachrichten*, 332, 859
- Hackman, T., Pelt, J., Mantere, M. J., et al. 2013, *A&A*, 553, A40
- Hall, D. S. 1983, *International Amateur-Professional Photometric Photometry Communications*, 13, 6
- Helfand, D. J., Schnee, S., Becker, R. H., White, R. L., & McMahon, R. G. 1999, *AJ*, 117, 1568
- Henry, G. W. 1999, *PASP*, 111, 845
- Horne, J. H. & Baliunas, S. L. 1986, *ApJ*, 302, 757
- Jetsu, L. 1996, *A&A*, 314, 153
- Jetsu, L., Hackman, T., Hall, D. S., et al. 2000, *A&A*, 362, 223
- Jetsu, L. & Pelt, J. 1996, *A&AS*, 118, 587
- Jetsu, L. & Pelt, J. 1999, *A&AS*, 139, 629
- Jetsu, L., Pelt, J., & Tuominen, I. 1993, *A&A*, 278, 449
- Kajatkari, P., Hackman, T., Jetsu, L., Lehtinen, J., & Henry, G. W. 2014, *A&A*, 562, A107
- Kajatkari, P., Jetsu, L., Cole, E., et al. 2015, *A&A*, 577, A84
- Koen, C. & Eyler, L. 2002, *MNRAS*, 331, 45
- Lacy, C. H. 1977, *ApJS*, 34, 479
- Lehtinen, J., Jetsu, L., Hackman, T., Kajatkari, P., & Henry, G. W. 2011, *A&A*, 527, A136
- Lehtinen, J., Jetsu, L., Hackman, T., Kajatkari, P., & Henry, G. W. 2012, *A&A*, 542, A38
- Lehtinen, J., Jetsu, L., Hackman, T., Kajatkari, P., & Henry, G. W. 2016, *A&A*, 588, A38
- Mitrou, C. K., Doyle, J. G., Mathioudakis, M., & Antonopoulou, E. 1996, *A&AS*, 115, 61
- Mohin, S. & Raveendran, A. V. 1987, *Journal of Astrophysics and Astronomy*, 8, 389
- Montes, D., Fernández-Figueroa, M. J., De Castro, E., et al.

- 2000, *A&AS*, 146, 103
- Pérez Martínez, M. I., Schröder, K.-P., & Cuntz, M. 2011, *MNRAS*, 414, 418
- Reinhold, T., Reiners, A., & Basri, G. 2013, *A&A*, 560, A4
- Rodonò, M., Messina, S., Lanza, A. F., Cutispoto, G., & Teriaca, L. 2000, *A&A*, 358, 624
- Roettenbacher, R. M., Monnier, J. D., Fekel, F. C., et al. 2015a, *ApJ*, 809, 159
- Roettenbacher, R. M., Monnier, J. D., Henry, G. W., et al. 2015b, *ApJ*, 807, 23
- Royer, F., Zorec, J., & Gómez, A. E. 2007, *A&A*, 463, 671
- Sato, K. & Kuji, S. 1990, *A&AS*, 85, 1069
- Simon, T. & Fekel, Jr., F. C. 1987, *ApJ*, 316, 434
- Stawikowski, A. & Glebocki, R. 1994, *Acta Astron.*, 44, 393
- Strassmeier, K. G., Fekel, F. C., Bopp, B. W., Dempsey, R. C., & Henry, G. W. 1990, *ApJS*, 72, 191
- Strassmeier, K. G., Hall, D. S., Boyd, L. J., & Genet, R. M. 1989, *ApJS*, 69, 141
- van Leeuwen, F. 2007, *A&A*, 474, 653
- Yoss, K. M. & Griffin, R. F. 1997, *Journal of Astrophysics and Astronomy*, 18, 161